Quantifying the trade-off between absolute capacity and rate-performance in battery electrodes

*Sang-Hoon Park, Ruiyuan Tian, João Coelho, Valeria Nicolosi, Jonathan N Coleman**

Dr. S. H. Park, Dr R. Tian, Dr J. Coelho, Prof. V. Nicolosi, Prof. J. N. Coleman

CRANN and AMBER research centers, Trinity College Dublin, Dublin 2, Ireland

E-mail: colemaj@tcd.ie

Dr. S. H. Park, Dr J. Coelho, Prof. V. Nicolosi

School of Chemistry, Trinity College Dublin, Dublin 2, Ireland

Dr R. Tian, Dr J. Coelho, Prof. J. N. Coleman

School of Physics, Trinity College Dublin, Dublin 2, Ireland

Keywords: (areal capacity, rate performance, power density, energy density)

ABSTRACT: Among other things, battery electrodes need to display large absolute capacities coupled with high rate-performance. However, enhancing areal capacity, for example *via* increased electrode thickness, results in reductions in rate-performance. This basis for this negative correlation has not been studied in a quantitative fashion. Here we use a semi-empirical model to analyse capacity *versus* rate data for electrodes fabricated from a number of materials, each measured at various thicknesses. Fitting the model to the data outputs the low-rate areal capacity, Q_A, and the characteristic time associated with charge/discharge, τ, fit parameters which quantify absolute capacity and rate performance respectively. We find a clear negative correlation between Q_A and τ, with all data siting close to a mastercurve approximately defined by constant τ/Q_A. This data is consistent with a simple model based on the timescales associated

with rate-limiting processes. This model implies that the capacity-rate trade-off can be improved for high areal capacity electrodes by increasing the volumetric capacity, electrical conductivity and porosity of the electrode. Conversely, solid-state diffusion and reaction kinetics are only important for low areal capacity electrodes.

1. Introduction

The needs of electric vehicles, coupled with the rapid rise of mobile electronics have made research into battery technologies increasingly important. [1, 2] Over the last decade, battery research has spanned a number of fields, from electrochemistry to nanotechnology.[2, 3] Although the dominant technology is still founded on the lithium-ion chemistry,[2, 4] cells based on storage of other ions such as sodium or aluminium are actively being studied.[5] Irrespective of the ions being stored, a common set of challenges will remain. Among other things, a high-performance battery will need to combine both high energy and power capabilities to meet the demands of the wide range of applications. In general, this is usually understood to mean that it is important to develop batteries with energy and power densities which are as high as possible.

To achieve these properties simultaneously, it will be necessary to fabricate electrodes with both large absolute capacity (represented by areal capacity, Q/A) and excellent rate-performance.[6, 7] The areal capacity of electrodes is important, not only because it determines the capacity of the cell, but also because it has a significant influence on the overall cell energy density. The reason for this is that, because the areal capacity of electrodes scales with thickness (see below), increasing areal capacity is generally achieved by increasing electrode thickness. As a result, the fraction of cell volume occupied by the electrodes increases, thus increasing the energy density. Recently, we demonstrated a simple model showing a monotonic relationship between electrode areal capacity and cell energy density such that the theoretical maximum

energy density can be approached at sufficiently high areal capacity.[8] This makes maximisation of areal capacity an important goal in battery research.

Because the areal capacity is given by $Q/A = L_E \times Q/V$, where L_E is the electrode thickness and Q/V is its measured volumetric capacity, maximisation of areal capacity requires combining high capacity materials with thick electrodes. However, it is well-known that thick electrodes tend to show reduced rate-performance such that there is clearly a trade-off between high absolute capacity and high rate-performance.[9-11]

A number of papers have attempted to characterize this trade-off.[10, 11, 12] While there is some understanding about the factors affecting the trade-off, there has been no quantitative analysis on what parameters are most relevant to the simultaneously maximisation of capacity and rate-performance. What is required is a quantitative understanding of the relationship between absolute capacity and rate-performance, including the effect of intrinsic properties, such as electrode conductivity and volumetric capacity, as well as extrinsic properties, such as electrode and separator thicknesses. Such an understanding would allow the tuning of parameters, in order to simultaneously maximise both capacity and rate-performance, leading to improved electrode performance.

Recently, we have developed a simple model to fit capacity *versus* rate data yielding the low-rate areal capacitance, Q_A, and the characteristic time associated with charge/discharge, τ, as fit parameters.[13] Together, these parameters describe the combination of areal capacity and rate-performance in battery electrodes. Here, we use this model to analyse data for a range of electrodes, fabricated from different materials at various thicknesses. Comparison of Q_A and τ, yields an improved understanding of the capacity-rate trade-off. We then use a simple physical model to examine the relationship between τ and Q_A, finding very good agreement with the experimental data. This combination of theory and experiment allows us to quantify the

physical parameters effecting τ and Q_A, and will allow performance optomisation *via* careful choice of both intrinsic and extrinsic properties.

2. Results and Discussion

2.1. Basic Characterization

To investigate the relationship between areal capacity (*Q/A*) and rate-performance over a wide range of areal capacities, we studied four different active materials with a range of theoretical specific capacities ($Li_4Ti_5O_{12}$, LTO=175 mAh g^{-1}, $LiNi_{0.5}Mn_{0.3}Co_{0.2}O_2$, NMC=165 mAh g^{-1}, $LiNi_{0.815}Co_{0.15}Al_{0.035}O_2$, NCA=190 mAh g^{-1}, and graphene-wrapped silicon, Gr-Si=2000 mAh g^{-1}, see SI for more information).[7, 13, 14] In each case, electrodes were fabricated using carbon nanotubes (CNT) as both binder and conductive additive (see Experimental Section) as this strategy is known to facilitate high areal capacities.[8] Nanotubes have significant advantages over traditional binder/additive systems in that they yield very good conductivity coupled with excellent mechanical robustness.[15] Shown in Figure 1A are representative SEM images of composite electrodes prepared from each active materials showing continuous nanotube networks. For each material (Figure 1B), a series of electrodes were produced with a broad range of mass loadings (*M/A*) and thicknesses (L_E). Such composites yield porous electrodes with a range of average densities (ρ_{LTO}=0.8 g cc^{-1}; ρ_{NMC}=2.0 g cc^{-1}; ρ_{NCA}=3.2 g cc^{-1}, and $\rho_{Gr\text{-}Si}$=0.4 g cc^{-1}).

For each material, electrochemical characterisation was performed for all loadings at a range of currents using CR2032 coin cells in a half-cell configuration. Shown in Figure 1C-F are representative charge-discharge curves measured at low rate (~1/10−1/20 C) for a number of electrode mass loadings for each active material. All electrodes display the characteristic voltage profiles associated with each material while the achieved areal capacities (*Q/A*) vary

over a wide range. The *Q/A* of the electrodes ranged from 0.03 to 35 mAh cm^{-2}, which is broad enough for a comprehensive analysis. Shown in Figure 1G is the measured low-rate *Q/A* for each material plotted as a function of electrode loading. In all cases, *Q/A* scaled linearly with *M/A*, indicating good electrolyte penetration into the porous electrodes (Figure 1G). The slope of the fit lines indicate average electrode specific capacities (*Q/M*, where *M* is total mass - active material and CNT). The electrodes display very high specific capacities (145, 162, 182 and 1960 mAh g^{-1} for LTO, NMC, NCA and Gr-Si electrodes, respectively), in all cases >80% of the theoretical capacity, confirming high electrochemical utilization, even at the reasonably high values of *M/A* under study.

2.2. Measuring Rate-Performance

For all electrodes, the rate-performance was characterized by performing galvanostatic charge/discharge experiments at a range of currents. Figure 2 shows the measured *Q/A* for each set of electrode plotted a function of rate, *R*. Here we define *R* as,

$$R = \frac{(I/A)}{(Q/A)_E} \approx 1/t_{\text{charge/discharge}} \quad (1)$$

where *I/A* is the applied areal current and $(Q/A)_E$ represents the experimentally-measured areal capacity (at a given areal current). As described previously,[13] we use this definition of rate, rather than *I/A* or C-rate because 1/*R* is a measure of charge/discharge time, allowing us to link the rate behaviour to physical parameters. In all cases, we find the expected behaviour where *Q/A* is constant at low rate but falls off as the rate exceeds a threshold value, $R_{90\%}$ (which we can define as the rate where the capacity reaches 90% of its maximum, low rate value). For each material, as the electrode mass loading is increased, two main effects occur. Firstly, the low-rate *Q/A* increases steadily with *M/A* as was shown in Figure 1F, indicating that more charge can be stored in thicker electrodes. Conversely, the threshold rate, $R_{90\%}$, decreases with increasing thickness, indicating poorer rate-performance at higher electrode thickness. Thus,

increasing electrode thickness results in both positive and negative outcomes. While both effects are commonly observed and neither is surprising, we know of no reports which quantitatively analyse the trade-offs associated with these phenomena.

In order to quantitatively analyse this behaviour, we need a metric for rate-performance. Recently, we showed that such a metric could be obtained by fitting capacity-rate data using the following semi-empirical model:

$$\frac{Q}{A} = Q_A\left[1-(R\tau)^n\left(1-e^{-(R\tau)^{-n}}\right)\right] \quad (2)$$

Here, Q_A is the low-rate areal capacity while τ is the characteristic time associated with charge/discharge. Very crudely, τ can be thought of as the minimum time required to charge an electrode to maximum capacity. In addition, n is a constant which generally lies in the range $0.5<n<1$ and depends on the rate-limiting mechanism such that values of $n\sim0.5$ are indicative of diffusive limitations where $n\sim1$ is thought to be associated with resistive limitations.[13, 16]

However, of these parameters, probably the most important is τ, simply because it is a direct measure of the critical rate, $R_{90\%}$, above which capacity starts to fall with rate. Using equation 2, this parameter can be found by taking the limit of low rate where the exponential disappears, such that:

$$R_{90\%} = (1/10)^{1/n} / \tau \quad (3)$$

Thus τ can be used as a metric for rate-performance, with smaller values of τ indicating better performance. Depending on the details of the electrode, τ has been observed to span a very wide range from $\sim1-10^4$ s and, as we will describe below, can be linked to electrode properties *via* rate limiting mechanisms.[13]

2.3. Analysing Rate-Performance

We have used equation 2 to fit each capacity-rate curve for all materials as shown in Figure 2. In all cases very good fits were obtained and values of Q_A, τ and n were extracted. All n values lay between 0.3 and 2 with the majority in the range 0.5−1.0 indicating the rate-performance to be predominately limited by a combination of diffusive and electrical effects. Perhaps more interesting are Q_A and τ which are plotted *versus* electrode thickness, L_E, for each material in Figure 3. In all cases, we find the low-rate areal capacity, Q_A, to increase linearly with electrode thickness, consistent with $Q_A = Q_V L_E$, where Q_V is the low-rate volumetric capacity (Figure 3, top row). From the slopes, we find Q_V-values of 110, 320, 560 and 750 mAh cm^{-3} for LTO, NMC, NCA and Gr-Si electrodes, respectively.

Perhaps more interesting is the scaling of τ with electrode thickness (Figure 3, bottom row). In all cases, we see a super-linear increase in τ with L_E, consistent with a significant reduction in rate-performance with increasing electrode thickness. This behaviour has its origin in that fact that the timescales associated with both charge and ion motion increase with electrode thickness leading to reduced rate-performance. Recently, we have proposed a simple model which relates τ to the mechanisms limiting charge/ion motion leading to an equation for τ as a function of the various physical properties of the electrode/electrolyte system:[13]

$$\tau = L_E^2\left[\frac{C_{V,eff}}{2\sigma_E}+\frac{C_{V,eff}}{2\sigma_{BL}P_E^{3/2}}+\frac{1}{D_{BL}P_E^{3/2}}\right]+L_E\left[\frac{L_S C_{V,eff}}{\sigma_{BL}P_S^{3/2}}\right]+\left[\frac{L_S^2}{D_{BL}P_S^{3/2}}+\frac{L_{AM}^2}{D_{AM}}+t_c\right] \qquad (4a)$$

where $C_{V,eff}$ is the effective volumetric *capacitance* of the electrode (F m^{-3}), σ_E is the out-of-plane electrical conductivity of the electrode material (S m^{-1}), σ_{BL} is the overall (anion and cation) conductivity of the bulk electrolyte (S m^{-1}), D_{BL} is the diffusion coefficient of Li ions in the bulk electrolyte (m^2 s^{-1}), P_E and P_S are the porosities of the electrode and separator respectively while L_S is the separator thickness (m). In addition, L_{AM} is a measure of the size of the active particles (m); D_{AM} is the solid state Li ion diffusion coefficient within the particles

(m^2/s) while t_c is a measure of the timescale associated with the electrochemical reaction once electron and ion combine at the active particle (s). This equation has been shown to accurately describe a wide range of experimental data and makes predictions which are consistent with observations.[13] We note that, applied to half-cells, this equation effectively ignores the lithium counter electrode. This is possible because lithium adsorption/desorption should occur exclusively at the metal surface and so occur on a timescale which is very short compared to all terms in equation 4a.

In its simplest form, this equation predicts τ to scale quadratically with L_E:

$$\tau = aL_E^2 + bL_E + c \qquad (4b)$$

where *a*, *b* and *c*, are defined in equation 4a. As shown in Figure 3 (bottom row), equation 4b fits all four data sets well with the fit parameters given in the panels. It is worth noting that, for NMC, NCA and SiGr, the fit returns *c* as zero within error, while for LTO *c* is quite small (3.6s). However, this does not actually mean that *c*=0 for NMC, NCA or SiGr. Instead, it implies relatively small values of *c* for these materials such that the data set is not extensive enough to yield *c* accurately. Nevertheless, this does imply that the last three terms in equation 4a are not significant under the circumstances of the electrodes under study here. As described in ref [13], these terms describe ion diffusion with both separator and active particles as well as the timescale associated with the electrochemical reaction. Because these contributions can be neglected for these specific electrodes, equation 4a implies that, under these circumstances, rate-performance is limited by a combination of the overall electrical resistance of the cell and ion diffusion in the electrolyte within the porous interior of the electrode.

2.4. Examining the Capacity Rate Trade-off

Because τ is a metric for rate-performance (smaller τ represents better rate-performance) and the achievable areal capacity can be represented by Q_A, the data in Figure 3 can be used to

assess the trade-off between capacity and rate-performance in battery electrodes. To examine this, we plot τ *versus* Q_A for all four materials under study (Figure 4A). Interestingly, we find a roughly linear dependence with all data sets lying roughly on the same master curve. Although such linearity appears to contradict equations 4a-b, as we shall see below, this is not the case. This graph illustrates the capacity-rate trade-off well. Ideally, an electrode material which combines high capacity with good rate-performance would have high Q_A but low τ. Figure 4A shows such a combination cannot be achieved, at least using the materials under study.

The approximate linearity shown in Figure 4A means that the slope of the master curve (i.e. τ/Q_A) is important: a lower slope would result in reduced τ for a given Q_A, and hence better rate-performance for a given areal capacity. As a result, we can use τ/Q_A as a measure of the capacity-rate trade-off. To explore this we plot τ/Q_A *versus* Q_A in Figure 4B. Here we find that τ/Q_A is not quite constant but has a relatively weak but well-defined dependence on Q_A, which we can show is a manifestation of equations 4a-b. To demonstrate this, we can combine equation 4b with $Q_A = Q_V L_E$ to give

$$\frac{\tau}{Q_A} = \frac{aQ_A}{Q_V^2} + \frac{b}{Q_V} + \frac{c}{Q_A} \qquad (5)$$

A plot of equation 5 on Figure 4B using the fit parameters from Figure 3 for LTO, shows good agreement while reasonable agreement is also found for the other materials as shown in figure S1, we don't plot the curves here to avoid clutter).

However, what is the most interesting about Figure 4B is that even though the data follows the expected Q_A-dependence, the curves for each material are shifted horizontally from each other such that the data as a whole lies in a narrow range of τ/Q_A roughly between 0.01 and 0.1 $cm^2\,mA^{-1}$. This can be seen more clearly by replotting the data in Figure 4B in Figure 4C on an expanded scale such that the vertical and horizontal ranges are equivalent (i.e. a range of $\times 10^4$).

In addition, we include an additional 70 data points found from fitting literature data to equation 2 (see Table 1 in SI). While the entire data set spans almost four orders of magnitude in Q_A, the majority of the data is constrained to a much narrower τ/Q_A range of just one decade. To illustrate this, we have plotted all the τ/Q_A data from Figure 4C (ours and literature) as a histogram in Figure 4C inset. This clearly shows a predominance of electrodes which display τ/Q_A between 0.01 and 0.1 $cm^2\,mA^{-1}$. This is important as it suggests that, in practice, there is limited scope to vary τ/Q_A, making it hard to improve rate-performance and absolute capacities simultaneously.

We believe the limited observed range for τ/Q_A is due to the relatively narrow range of properties associated with the electrode/electrolyte system in lithium ion batteries. To demonstrate this, we combined equation 4a with $Q_A = Q_V L_E$ to give an equation for τ/Q_A in terms of a range of parameters representing electrode/electrolyte properties, including Q_A.

$$\frac{\tau}{Q_A} = \frac{Q_A}{Q_V}\left[\frac{C_{V,eff}/Q_V}{2\sigma_E} + \frac{C_{V,eff}/Q_V}{2\sigma_{BL}P_E^{3/2}} + \frac{1}{D_{BL}P_E^{3/2}Q_V}\right] + \left[\frac{L_S C_{V,eff}/Q_V}{\sigma_{BL}P_S^{3/2}}\right] + \frac{1}{Q_A}\left[\frac{L_S^2}{D_{BL}P_S^{3/2}} + \frac{L_{AM}^2}{D_{AM}} + t_c\right] \quad (6)$$

We can use this equation to simulate the τ/Q_A *versus* Q_A results in Figure 4C. To do this, we note that, in addition to our data, figure 4C includes data for a number of other research groups, measured on broad range of electrodes fabricated from various materials. We can model such data by calculating τ/Q_A for a range of electrode/electrolyte combinations, described by a set of physical properties (i.e. those described by equation 6), which can vary somewhat depending on the details of the electrode/electrolyte system. To perform the simulation, Q_V, σ_E, P_E, L_{AM}, D_{AM} and t_c were chosen randomly within certain physically reasonable ranges (see Figure 4 caption for ranges). In addition, we used fixed values of σ_{BL}=1 S m^{-1}, D_{BL}=5×10^{-10} $m^2\,s^{-1}$, P_s=40%, L_S=25 μm as these properties have little scope to vary in typical experiments. Finally, we chose $C_{V,eff}/Q_V = 28$ F mAh^{-1} based on our recent results.[13] Using these data sets as input

values, we calculated values of τ/Q_A for a range of Q_A values between 0.01 and 100 mAh cm^{-2} as shown in Figure 4D (see table 3 in SI for more detail).

We found the simulated values of τ/Q_A to match the experimental data in Figure 4C very well. The simulated data show a well-defined minimum which depends weakly on Q_A but no clear upper limit. The envelope describing the minimum observed values of τ/Q_A can be found simply by inserting extreme values from each property range into equation 6 (for example using the highest values of Q_V, σ_E, P_E and D_{AM} but the lowest values of L_{AM} and t_c). This minimum curve is plotted as a function of Q_A in Figure 4D and provides a clear lower bound to the simulated data. This curve has been reproduced on Figure 4C and also provides a reasonable lower bound to the experimental data with only a few data points lying below it.

We can understand the simulated data in Figure 4D more clearly by plotting it as a histogram in Figure 4D inset. This histogram is very similar to that in Figure 4C (inset), showing a clear peak in τ/Q_A between ~0.01 and 0.1 cm^2 mA^{-1}. This shows equation 5 (and by implication equation 4a) to be able to quantitatively describe experimental data.

2.5. Optimised Charging Currents

Below, we will use equation 6 to explore how best to simultaneously maximise rate-performance and areal capacity. However, first, we make an interesting observation. The data in Figure 4 C-D suggests battery electrodes to show values of τ/Q_A which fall in a relatively limited range. Rate measurements are usually made by charging or discharging an electrode at a constant current density. Above some current density, the achievable capacity tends to fall off. One way to quantify when this fall-off begins would be *via* the current density which yields 90% of the low-rate capacity. Rewriting equation 1, this would be $(I/A)_{90\%} = R_{90\%} \times 0.9Q_A$ where the low-rate areal capacity is represented by Q_A. Then using equation 3, we can write

$$(I/A)_{90\%} = 0.9 \times (1/10)^{1/n} Q_A / \tau \qquad (7)$$

This equation links $(I/A)_{90\%}$, which can be considered the largest current density which yields close to maximal capacity, to the fit parameters obtained from fitting capacity *versus* rate data using equation 2. Interestingly, equation 7 implies that, because τ/Q_A values fall in a relatively limited range, then $(I/A)_{90\%}$ values should also be quite similar over a range of materials. To test this, we used the Q_A, τ and n data obtained from fitting our data as a well as the literature data shown in Figure 4C to calculate $(I/A)_{90\%}$ using equation 7. The data are presented as a histogram in Figure 4E. Clearly, much of this data is concentrated between roughly 0.5 and 5 mA cm^{-2}, which is a relatively narrow range. This could be a useful tool to aid researchers performing rate studies in deciding what currents to use to gather data both in the low-rate, constant capacity regime ($I/A < (I/A)_{90\%}$) as well as the high-rate, decreasing capacity regime ($I/A > (I/A)_{90\%}$).

To confirm this, we searched the literature for rate data which unambiguously showed both regimes (See Table 2 in SI).[11, 12, 17] In each case, we extracted $(I/A)_{90\%}$ directly from the graphs, plotting the data as a histogram in Figure 4F. This plot shows a clear peak in $(I/A)_{90\%}$ between 1 and 6 mA cm^{-2}, in good agreement with the fit data. This supports the idea that the $(I/A)_{90\%}$ is roughly constant across all materials.

2.6. How to Simultaneously Optimise Capacity and Rate Behaviour

Given that equation 6 appears to accurately describe experimental data, we can use it to explore the effect of various parameters on capacity/rate behaviour. We do this by plotting τ/Q_A *versus* Q_A for various combinations of electrode/electrolyte properties in Figure 5. We note that lower values of τ/Q_A represent a better trade-off between areal capacity and rate-performance. In each panel, we used fixed values of σ_{BL}=1 S m^{-1}, D_{BL}=5×10^{-10} m^2 s^{-1}, P_s=40%, L_S=25 μm and

$C_{V,eff} / Q_V$ =28 F mAh^{-1} as before. In addition, the black curve in each plot uses the values: Q_V=3×10^9 mAh m^{-3}; σ_E=30 S m^{-1}; P_E=70%; L_{AM}=50 nm; D_{AM}=10^{-12} m^2 s^{-1}; t_c=0.1 s and approximates the lower limit for τ/Q_A. In each panel, all but one of these parameters are kept constant and the remaining parameter varied in such as to increase τ/Q_A from its lower boundary. The top panels (Figure 5 A-C) show the dependence of τ/Q_A on volumetric capacity, Q_V as well as electrode conductivity, σ_E, and porosity, P_E. While none of these parameters significantly affect τ/Q_A for low values of Q_A, all three have a significant effect at high values of Q_A. This emphasises the importance of these parameters to high capacity electrodes. In particular, Q_V has a large impact on the high-Q_A performance. We believe this is a very important insight, which can be understood quite simply: if Q_V is large, a given Q_A can be achieved at relatively low electrode thickness. This boosts rate-performance by reducing parameters such as the time for ions to diffuse through the porous interior of the electrode. The beneficial effect of high Q_V is particularly important, as high performance electrodes (i.e. those with high Q_V) should yield the best possible combination of areal capacity and rate.

We can also use these concepts to explore the effect of calendaring on rate performance. Calendaring is effectively a densification process which reduces the thickness of the electrode, eliminating porosity and in effect increasing the volumetric energy density. As shown in figure 5C, such a porosity reduction appears to disimprove the capacity-rate tradeoff by increasing τ/Q_A for high Q_A-electrodes. However, in line with figure 5A, the commensurate increase in Q_V will simultaneously decrease τ/Q_A, compensating for the porosity reduction. Thus, we might expect calendaring not to have a significant negative effect on the capacity-rate tradeoff while improving energy density *via* the increase in Q_V.

In addition, the bottom panels (Figure 5 D-F) show the dependence of τ/Q_A on particle size, L_{AM}, and diffusion coefficient, D_{AM}, as well as reaction time, t_c. In contrast to the top panels,

varying these parameters tends to predominately effect τ/Q_A at low values of Q_A. The reason for this is also simple. These parameters describe processes (solid-state diffusion and reaction kinetics) which do not depend on electrode thickness. Thus, while their contribution to the time constant is significant for thinner, low-Q_A electrodes, once electrode thickness become large, as would be the case in high-Q_A systems, solid-state diffusion times and reaction times become small compared to the time for an ion to diffuse through the porous interior of the electrode.

The concepts described above allow us to make some points about simultaneously maximising areal capacity and rate-performance. Firstly, throughout the literature, solid-state diffusion is often cited as the dominant factor limiting rate-performance in battery electrodes.[14, 18] A good example of this would be the utilisation of lithium titanate as a high-rate anode due to its high solid-state diffusion coefficient.[14, 19] However, as electrodes get thicker to increase the areal capacity, the time associated with solid state diffusion becomes very small compared to the time associated with diffusion of ions through the porous electrolyte. This has been clearly demonstrated in a number of papers.[13, 20] Thus for thicker electrodes, designed to maximise areal capacity but where the rate-performance needs to be as good as possible, it is much more important to have Q_V as high as possible than it is to have high D_{AM}.

One can make a similar argument about using nano-structured electrode materials to maximise rate-performance as has been proposed on a number of occasions.[9, 21] Figure 5D shows reducing particle size (L_{AM}) to improve the trade-off between areal capacity and rate-performance by yielding lower τ/Q_A, but only at low values of Q_A. For higher values of Q_A, the areal capacity-rate trade-off is quite insensitive to L_{AM} for the reasons described above. In fact, electrodes made from particles with somewhat larger L_{AM} could have lower porosity leading to higher Q_V. This would lead to a better capacity/rate trade-off at high Q_A. We note that this argument does not mean that nano-particles do not confer some advantages. Clearly they do,[22] not least in terms of processing, stability etc. For example, exfoliated 2D nanosheets are more

easily processed[23] and much more stable as electrode materials than the associated bulk powder.[24] In addition, nano-sized Si particles tend to be much more stable against pulverisation than micron-sized Si particles.[8] However, it is important to assess the overall effect of size, especially when considering rate-performance.

2.7. Optimising Electrode Thickness

The data in figure 4 and 5 for LTO shows τ/Q_A to display a minimum when plotted versus Q_A. Similarly, as $Q_A = Q_V L_E$, this implies there is an optimum electrode thickness where τ/Q_A is minimised, representing the best possible trade-off between capacity and rate. This can be demonstrated by rewriting equation 5 as a function of L_E:

$$\frac{\tau}{Q_A} = \frac{aL_E}{Q_V} + \frac{b}{Q_V} + \frac{c}{Q_V L_E} \tag{8a}$$

This equation represents a "U-shaped" curve when plotted versus L_E. The electrode thickness associated with the minimum value of τ/Q_A can be found by differentiating and setting $d(\tau / Q_A)/dL_E = 0$, yielding an optimum electrode thickness:

$$L_{E,OP} = \sqrt{c/a} = \left[\frac{\frac{L_S^2}{D_{BL} P_S^{3/2}} + \frac{L_{AM}^2}{D_{AM}} + t_c}{\frac{C_{V,eff}}{2\sigma_E} + \frac{C_{V,eff}}{2\sigma_{BL} P_E^{3/2}} + \frac{1}{D_{BL} P_E^{3/2}}} \right]^{1/2} \tag{8b}$$

where we use the definitions of *a* and *c* from equations 4a and b. This equation can be used to estimate the optimum electrode thickness once the relevant physical properties of the system are known. It should be noted that, although the data-fitting described above yielded values of $c \approx 0$, as discussed previously this does not mean that *c* is exactly equal to zero. In real batteries, *c* will always have a non-zero value and in some cases might be significant. For example, fitting

data for micron-sized silicon has yielded c=2027 s.[13] Thus, in any real situation $L_{E,OP}$ will be non-zero.

Clearly, not all of the terms in equation 8b are important for a given situation. For example, we have argued previously that,[13] the middle term in the denominator will often be dominant whilst in the numerator, it might be expected that solid state diffusion term (middle term) will usually be the most important of the three. Then, we can make the approximation that, under such circumstances the optimum electrode thickness can be approximated by

$$L_{E,OP} \approx \left[\frac{2\sigma_{BL} P_E^{3/2} L_{AM}^2}{D_{AM} C_{V,eff}} \right]^{1/2} \qquad (8c)$$

We can plot this equation as a contour graph (figure 6) to give $L_{E,OP}$ plotted as a function of both Q_V and the solid-state diffusion time, L_{AM}^2 / D_{AM} . Such data will allow thickness optimisation for a given electrode material (represented by Q_V and L_{AM}^2 / D_{AM}). We believe equations 8a-c will be useful in deciding the thickness of electrodes in cell stacks where combinations of high capacity and rate are important.

Finally, we would like to make what we believe is an important general point. Many papers assess rate-performance *via* comparisons of specific capacity (i.e. capacity per unit mass). We believe this is incorrect. For practical batteries, the absolute capacity is important which depends on both specific capacity and electrode thickness (achieving high specific capacity in thin electrodes is straightforward, however, achieving this in thick electrodes is much harder). We have shown here that there is a clear negative correlation between areal capacity and rate-performance, leading to the trade-off discussed above. This trade-off means the ubiquitous reduction in capacity with rate occurs at lower rates for the thicker the electrode (and so the higher the low-rate capacity). However, another effect, which we have not yet mentioned, is also important. For thick electrodes, although the capacity starts to fall off at lower rates

compared to thin electrodes, it falls from a much higher baseline (due to the higher low-rate capacity). The resultant performance can only be assessed by examining the absolute (i.e. the areal) capacity. Comparisons using absolute capacity can avoid overly optimistic evaluation of the rate-performance that may not be implementable in commercial batteries.

3. Conclusion

In conclusion, we have measured the areal capacity as a function of rate for four different electrode materials, each at a range of electrode thicknesses. In each case, using a semi-empirical equation, we have fitted capacity/rate data, obtaining the low-rate capacity and characteristic time as fit parameters. In addition, we performed similar analysis on a number of data sets extracted from the literature. Because these parameters represent the achievable capacity and rate-performance respectively, we can use this data to assess relationship between areal capacity and rate-performance.

In all cases, we find a trade-off between areal capacity and rate-performance, such that increasing areal capacity, for example by increasing electrode thickness, results in reduced rate-performance. However, we find the data to be consistent with a simple model, a factor which is important as it allows us to identify the parameters which control how rapidly rate-performance degrades as areal capacity is increased. As a result, we find that the capacity-rate trade-off can be improved for high areal capacity electrodes by increasing the volumetric capacity, electrical conductivity and porosity of the electrode. Conversely, factors such as solid-state diffusion coefficient, particle size and reaction kinetics are important for low areal capacity electrodes. These results challenge a number of paradigms in battery research.

4. Experimental Section

All the electrodes were prepared by a conventional slurry-casting method using a single walled carbon nanotube (SWCNT) aqueous dispersion (0.2 wt% SWCNT in water, ~0.2 wt%

polyvinylpyrrolidone (PVP) as a surfactant, Tuball, OCSiAl). The active material powder was mixed with the CNT dispersion to form uniform slurry by using a mortar and pestle. For more comprehensive analysis, here we used various types of the active materials, such as LTO ($Li_4Ti_5O_{12}$, 100 nm size, Sigma-Aldrich), NMC (NMC_{532}, MTI Corp.), NCA (Ni:Co:Al = 8.15:1.5:0.35, MTI Corp.), and Gr-Si (Nano GCA-2000, Angstron Materials). For each active materials, different CNT M_f were introduced (LTO: 7.5 wt%, NMC: 0.5 wt%, NCA: 0.5 wt%, and Gr-Si: 4 wt%, respective), which were the optimized conditions in our previous study. The uniformly mixed slurry was then coated onto the current collector (either Cu or Al foil) using a doctor blade. Here, the thickness of electrodes were controlled (or electrode areal mass loading, M/A) by varying the doctor blade height. The electrodes were dried at an ambient condition for 2 hours and followed by vacuum drying at 100 °C for 12 hours.

The electrochemical properties were measured in 2032-type coin cells (MTI Corp.). We used punched discs (d= 1.2 cm, and A=1.13 cm^2) as the working electrode. We used Celgard 2320 as the separator and 1.2 M $LiPF_6$ in ethylene carbonate/diethyl carbonate/fluoroethylene carbonate (EC/DEC/FEC, 3:6:1 in v/v/v, BASF) with 2 wt% vinylene carbonate (VC, Sigma Aldrich) as the electrolyte. The coin cells were assembled in an Ar-filled glovebox (UNIlab Pro, Mbraun) with using Li-metal as a counter electrode. The electrochemical properties of the cells were measured using Galvanostatic charge/discharge test by a potentiostat (VMP3, Biologic). The maximum capacity of the electrodes were investigated at a reasonably slow condition of ~1/10−1/20 C-rate. Then rate-performance was measured by asymmetric charge/discharge protocol; the cells were charged at a fixed rate of ~1/20 C then discharged at various rates.

Supporting Information

Supporting Information is available from the Wiley Online Library or from the author.

Acknowledgements

Dr. S. H. Park, Dr R. Tian, and Dr J. Coelho contributed equally to this work. All authors acknowledge the SFI-funded AMBER research centre (SFI/12/RC/2278) and Nokia for support. JNC thanks Science Foundation Ireland (SFI, 11/PI/1087), the Graphene Flagship (grant agreement n°785219) and the ERC (Adv. Gr. FUTUREPRINT) for funding. VN thanks the European Research Council (SoG 3D2D Print) and Science Foundation Ireland (PIYRA) for funding.

Received: ((will be filled in by the editorial staff))

Revised: ((will be filled in by the editorial staff))

Published online: ((will be filled in by the editorial staff))

References

[1] Z. P. Cano, D. Banham, S. Y. Ye, A. Hintennach, J. Lu, M. Fowler, Z. W. Chen, *Nature Energy*, **2018**, *3*, 279; Y. L. Cao, M. Li, J. Lu, J. Liu, K. Amine, *Nat. Nanotechnol.*, **2019**, *14*, 200.

[2] J. Lu, Z. H. Chen, Z. F. Ma, F. Pan, L. A. Curtiss, K. Amine, *Nat. Nanotechnol.*, **2016**, *11*, 1031.

[3] V. Etacheri, R. Marom, R. Elazari, G. Salitra, D. Aurbach, *Energy Environ. Sci.*, **2011**, *4*, 3243; J. B. Goodenough, *Acc. Chem. Res.*, **2013**, *46*, 1053.

[4] B. Dunn, H. Kamath, J. M. Tarascon, *Science*, **2011**, *334*, 928.

[5] R. C. Masse, E. Uchaker, G. Z. Cao, *Science China-Materials*, **2015**, *58*, 715; X. L. Ren, K. Turcheniuk, D. Lewis, W. B. Fu, A. Magasinski, M. W. Schauer, G. Yushin, *Small*, **2018**, *14*, 1703425 ; X. Q. Xie, T. Makaryan, M. Q. Zhao, K. L. Van Aken, Y. Gogotsi, G. X. Wang, *Adv. Energy Mater.*, **2016**, *6*; M. C. Lin, M. Gong, B. G. Lu, Y. P. Wu, D. Y. Wang, M. Y. Guan, M. Angell, C. X. Chen, J. Yang, B. J. Hwang, H. J. Dai, *Nature*, **2015**, *520*, 325.

[6] T. M. Higgins, S. H. Park, P. J. King, C. Zhang, N. McEvoy, N. C. Berner, D. Daly, A. Shmeliov, U. Khan, G. Duesberg, V. Nicolosi, J. N. Coleman, *ACS Nano*, **2016**, *10*, 3702.

[7] C. J. Zhang, S. H. Park, A. Seral-Ascaso, S. Barwich, N. McEvoy, C. S. Boland, J. N. Coleman, Y. Gogotsi, V. Nicolosi, *Nature Commun.*, **2019**, *10*, 849.

[8] S.-H. Park, P. J. King, R. Tian, C. S. Boland, J. Coelho, C. J. Zhang, P. McBean, N. McEvoy, M. P. Kremer, D. Daly, J. N. Coleman, V. Nicolosi, *Nature Energy*, **2019**, *DOI:10.1038/s41560-019-0398-y*.

[9] C. F. Zhang, S. H. Park, O. Ronan, A. Harvey, A. Seral-Ascaso, Z. F. Lin, N. McEvoy, C. S. Boland, N. C. Berner, G. S. Duesberg, P. Rozier, J. N. Coleman, V. Nicolosi, *Small*, **2017**, *13*, 1701677.

[10] Z. J. Du, D. Wood, C. Daniel, S. Kalnaus, J. L. Li, *J. Appl. Electrochem.*, **2017**, *47*, 405.

[11] K. G. Gallagher, S. E. Trask, C. Bauer, T. Woehrle, S. F. Lux, M. Tschech, P. Lamp, B. J. Polzin, S. Ha, B. Long, Q. L. Wu, W. Q. Lu, D. W. Dees, A. N. Jansen, *J. Electrochem. Soc.*, **2016**, *163*, A138; H. H. Zheng, J. Li, X. Y. Song, G. Liu, V. S. Battaglia, *Electrochim. Acta*, **2012**, *71*, 258.

[12] D. Y. W. Yu, K. Donoue, T. Inoue, M. Fujimoto, S. Fujitani, *J. Electrochem. Soc.*, **2006**, *153*, A835.
[13] R. Tian, S. H. Park, P. J. King, G. Cunningham, J. Coelho, V. Nicolosi, J. N. Coleman, *Nature Commun.*, **2019**, *10*, 1933.
[14] J. Coelho, A. Pokle, S. H. Park, N. McEvoy, N. C. Berner, G. S. Duesberg, V. Nicolosi, *Sci. Rep.*, **2017**, *7*, 7614.
[15] Y. P. Liu, X. Y. He, D. Hanlon, A. Harvey, U. Khan, Y. G. Li, J. N. Coleman, *ACS Nano*, **2016**, *10*, 5980.
[16] Z. Ling, A. Harvey, D. McAteer, I. J. Godwin, B. Szydlowska, A. Griffin, V. Vega-Mayoral, Y. C. Song, A. Seral-Ascaso, V. Nicolosi, J. Coleman, *Adv. Energy Mater.*, **2018**, *8*, 1702364.
[17] H. T. Sun, L. Mei, J. F. Liang, Z. P. Zhao, C. Lee, H. L. Fei, M. N. Ding, J. Lau, M. F. Li, C. Wang, X. Xu, G. L. Hao, B. Papandrea, I. Shakir, B. Dunn, Y. Huang, X. F. Duan, *Science*, **2017**, *356*, 599; R. Moshtev, B. Johnson, *J. Power Sources*, **2000**, *91*, 86; G. H. Lee, S. Lee, C. W. Lee, C. Choi, D. W. Kim, *J. Mater. Chem. C.*, **2016**, *4*, 1060; Z. M. Wan, J. Shao, J. J. Yun, H. Y. Zheng, T. Gao, M. Shen, Q. T. Qu, H. H. Zheng, *Small*, **2014**, *10*, 4975; K. Higa, S. L. Wu, D. Y. Parkinson, Y. B. Fu, S. Ferreira, V. Battaglia, V. Srinivasan, *J. Electrochem. Soc.*, **2017**, *164*, E3473; S. A. Kayser, A. Mester, A. Mertens, P. Jakes, R. A. Eichel, J. Granwehr, *Phys. Chem. Chem. Phys.*, **2018**, *20*, 13765; L. Leveau, B. Laik, J. P. Pereira-Ramos, A. Gohier, P. Tran-Van, C. S. Cojocaru, *J. Power Sources*, **2016**, *316*, 1; J. S. Sander, R. M. Erb, L. Li, A. Gurijala, Y. M. Chiang, *Nature Energy*, **2016**, *1*; S. Xu, C. M. Hessel, H. Ren, R. Yu, Q. Jin, M. Yang, H. Zhao, D. Wang, *Energy Environ. Sci.*, **2014**, *7*, 632; Y.-J. Han, J. Kim, J.-S. Yeo, J. C. An, I.-P. Hong, K. Nakabayashi, J. Miyawaki, J.-D. Jung, S.-H. Yoon, *Carbon*, **2015**, *94*, 432.
[18] W. B. Du, A. Gupta, X. C. Zhang, A. M. Sastry, W. Shyy, *Int. J. Heat Mass Transfer*, **2010**, *53*, 3552; L. Xue, X. P. Li, Y. H. Liao, L. D. Xing, M. Q. Xu, W. S. Li, *J. Solid State Electrochem.*, **2015**, *19*, 569.
[19] S. B. Yoon, H. K. Kim, K. C. Roh, K. B. Kim, *J. Electrochem. Soc.*, **2015**, *162*, A667.
[20] C. Heubner, J. Seeba, T. Liebmann, A. Nickol, S. Borner, M. Fritsch, K. Nikolowski, M. Wolter, M. Schneider, A. Michaelis, *J. Power Sources*, **2018**, *380*, 83; H. Gao, Q. Wu, Y. X. Hu, J. P. Zheng, K. Amine, Z. H. Chen, *J. Phys. Chem. Lett.*, **2018**, *9*, 5100.
[21] Y. G. Wang, H. Q. Li, P. He, E. Hosono, H. S. Zhou, *Nanoscale*, **2010**, *2*, 1294; G. Ali, S. A. Patil, S. Mehboob, M. Ahmad, H. Y. Ha, H. S. Kim, K. Y. Chung, *J. Power Sources*, **2019**, *419*, 229; T. Beuvier, M. Richard-Plouet, M. Mancini-Le Granvalet, T. Brousse, O. Crosnier, L. Brohan, *Inorg. Chem.*, **2010**, *49*, 8457.
[22] M. J. Armstrong, C. O'Dwyer, W. J. Macklin, J. D. Holmes, *Nano Res.*, **2014**, *7*, 1.
[23] V. Nicolosi, M. Chhowalla, M. G. Kanatzidis, M. S. Strano, J. N. Coleman, *Science*, **2013**, *340*, 1420.
[24] Y. D. Liu, L. Ren, X. Qi, L. W. Yang, J. Li, Y. Wang, J. X. Zhong, *Journal of Energy Chemistry*, **2014**, *23*, 207.

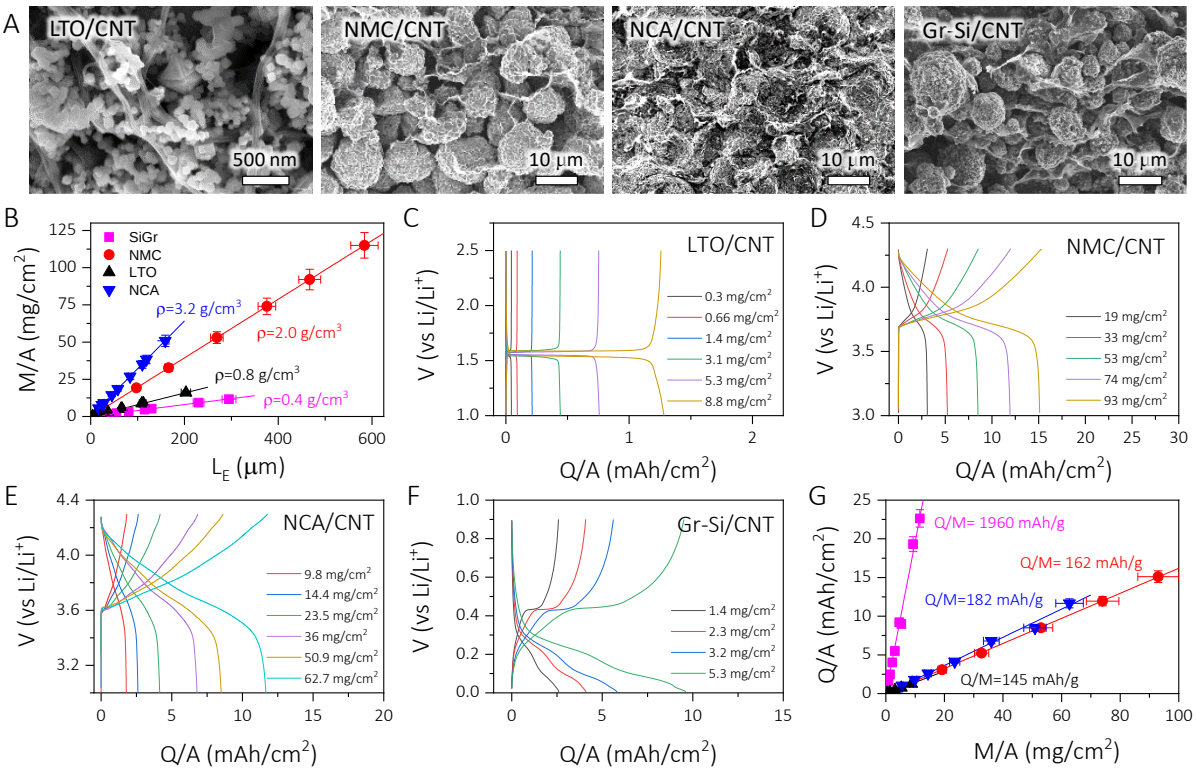

Figure 1. (A) SEM images for the composite electrodes prepared using various types of the active materials (LTO, NMC, NCA, and Gr-Si). B) Areal mass loading plotted *versus* electrode thickness for all materials. The slope of the fit lines give the mean electrode densities. C-F) Representative galvanostatic charge-discharge curves for (C) LTO/CNT, (D) NMC/CNT, (E) NCA/CNT, and (F) Gr-Si/CNT electrodes with different areal mass (M/A). Maximum areal capacities of the electrodes at the different M/A were measured at a reasonably slow condition of ~1/10−1/20 C-rate. (G) Q/A plotted as a function of M/A for various electrodes. Slope of the fit lines indicate the average electrode specific capacities (Q/M).

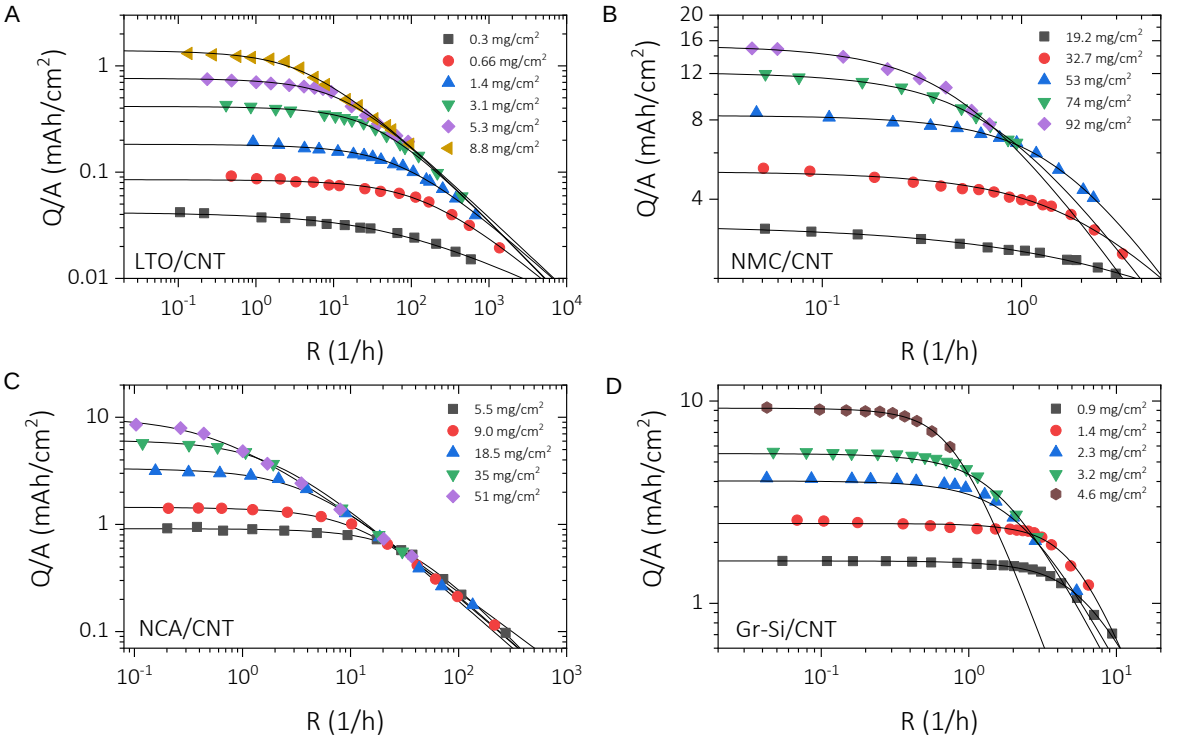

Figure 2. The rate-performances of the electrodes with varying the electrode areal mass. Areal capacity (Q/A) plotted as a function of rate, R, for a subset of electrodes with a range of M/A-values fabricated for (A) LTO/CNT, (B) NMC/CNT, (C) NCA/CNT, and (D) Gr-Si/CNT. M/A-values of the electrodes are indicated in the inset. The lines are fits to equation 2.

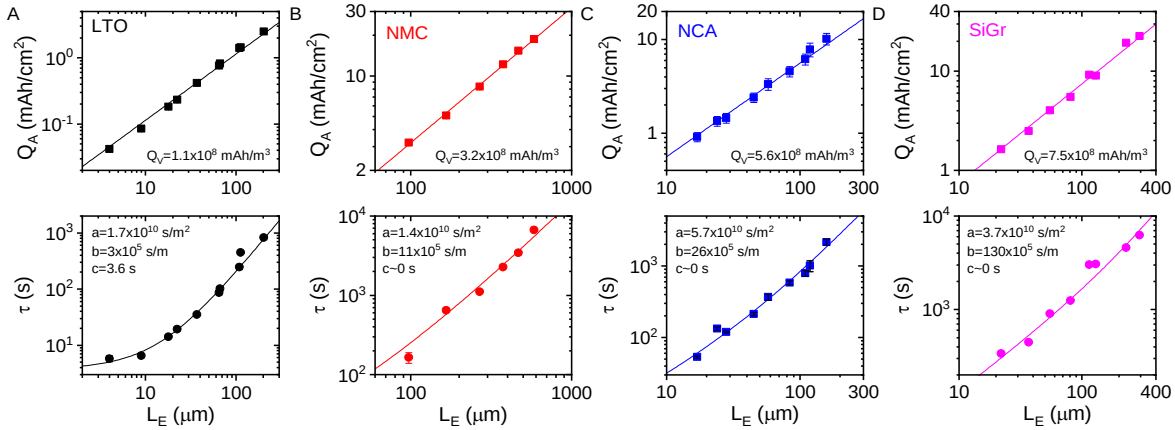

Figure 3. Fit parameters, Q_A (top row) and τ (bottom row), extracted from the rate curves in Figure 2, plotted *versus* electrode thickness, L_E, for A) LTO/SWCNT, B) NMC/SWCNT, C) NCA/SWCNT and D) Si-GR/SWCNT electrodes. The fits in the top and bottom rows are to $Q_A = Q_V L_E$ and equations 4b respectively. Fit parameters are given in the panels. N.B for NMC, NCA and SiGr, the fit gave values of *c* which were zero within error. In those cases, we have written *c*~0 to indicate that although *c* is not known accurately, it is relatively small.

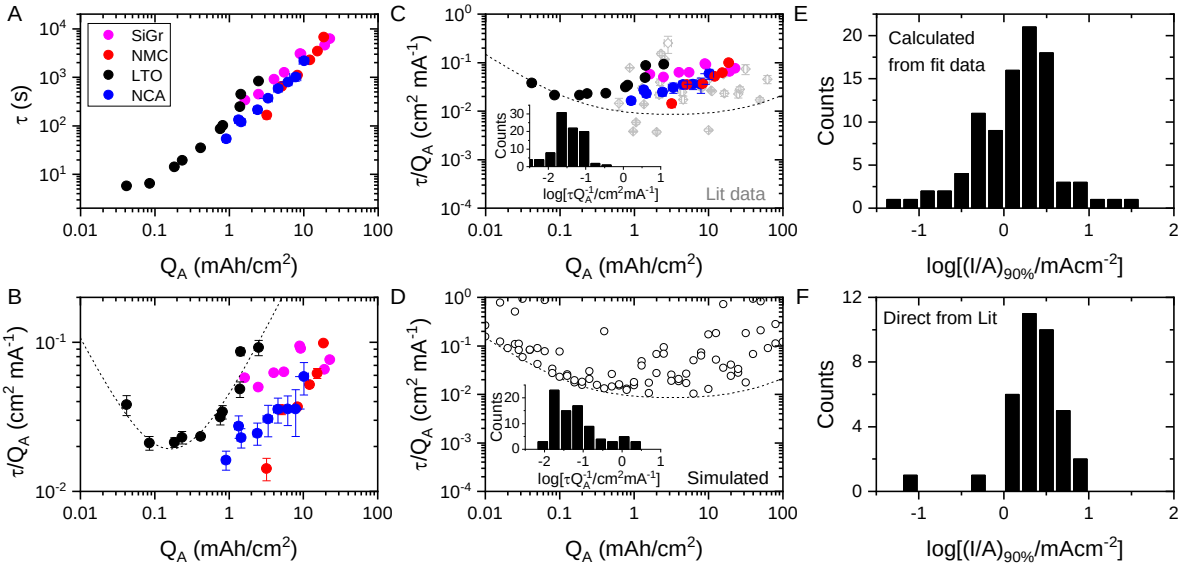

Figure 4. The relationship between rate-performance and absolute capacity. A) Plot of τ vs. Q_A for the electrodes fabricated in this study. B) Plot of τ/Q_A vs. Q_A for the electrodes fabricated in this work. The dashed line is a plot of equation 5 using the fit parameters given in figure 3A. C) The data for τ/Q_A reported in Figure 4B plotted on an expanded scale and including literature data for comparison (see SI). Inset: All data contained in this graph plotted as a histogram. D) Simulated plot of τ/Q_A vs. Q_A for electrodes with varying physical parameters. This data was generated using equation 6 using values of the following parameters chosen randomly from within the ranges given in brackets: Q_V (1×10^8–3×10^9 mAh m^{-3}); σ_E (0.1–30 S m^{-1}); P_E (30–70%); L_{AM} (50 nm–2 μm); D_{AM} (10^{-15}–10^{-12} m^2 s^{-1}); t_c (0.1–10 s). In addition, the fixed values σ_{BL}=1 S m^{-1}, $D_{BL}=5\times10^{-10}$ m^2 s^{-1}, P_s=40%, L_S=25 μm and $C_{V,eff}/Q_V = 28$ F mAh^{-1} were used. The dashed lines in C and D were plotted using equation 6 using the fixed values above and the extreme ends of the ranges which give the lowest τ/Q_A values. Inset: All data contained in this graph plotted as a histogram. E-F) Histograms showing the maximum practical

charging/discharging current (defined as the current which yields 90% of maximum capacity) found in 2 ways: E) calculated from the capacity-rate fit parameters and F) extracted directly from literature.

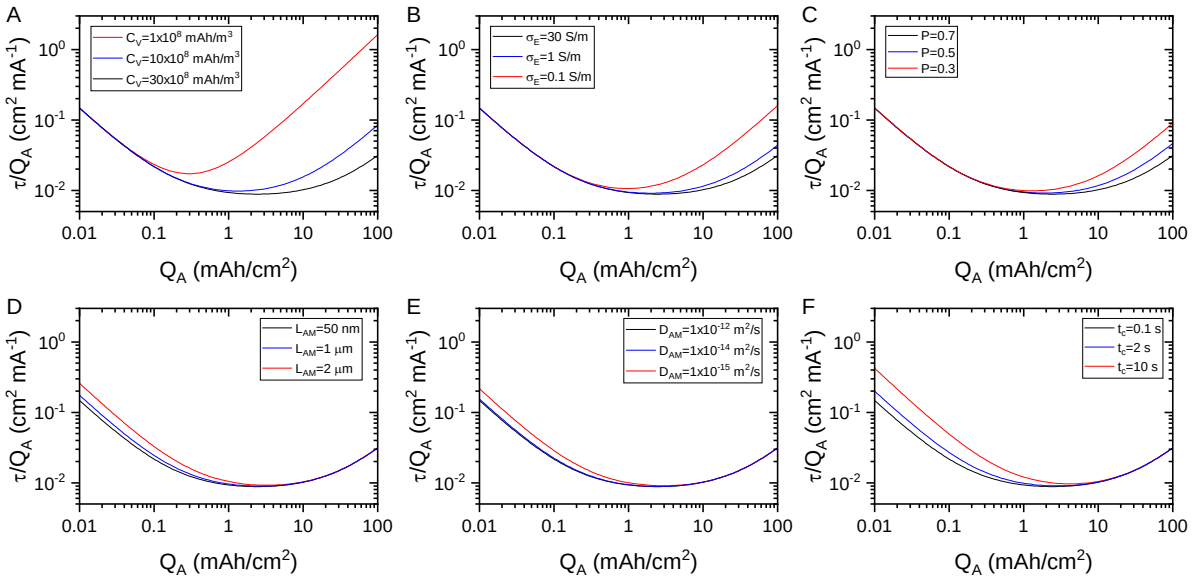

Figure 5. Dependence of τ/Q_A on Q_A, calculated using equation 6, while varying one parameter at a time. In all cases, fixed values σ_{BL}=1 S m^{-1}, D_{BL}=5×10^{-10} m^2 s^{-1}, P_s=40%, L_S=25 μm and $C_{V,eff}/Q_V$ =28 F mAh^{-1} were used with the other parameters varied systematically. When a given parameter was varied, all other parameters were held constant with values of: Q_V=3×10^9 mAh m^{-3}; σ_E=30 S m^{-1}; P_E=70%; L_{AM}=50 nm; D_{AM}=10^{-12} m^2 s^{-1}; t_c=0.1 s. We note that these values represent the limits of the ranges used in Figure 4D which minimise τ/Q_A. In all panels, the black curves use the parameters given above while the red and blue curves each vary one parameter in such a way as to increase τ/Q_A.

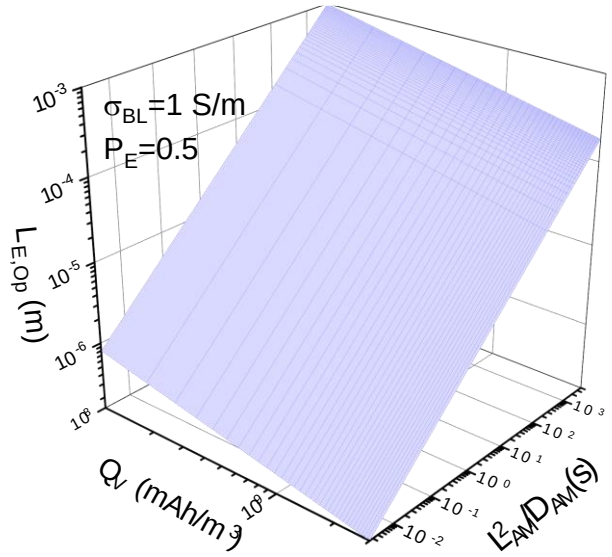

Figure 6. The optimum electrode thickness, $L_{E,Op}$, where the capacity/rate tradeoff is best (i.e. τ/Q_A is minimised) plotted as a function of Q_V and the solid state diffusion time, L_{AM}^2 / D_{AM}. This was computed using equation 8c, taking σ_{BL}=1 S/m, P_E=0.5 and using $C_{V,eff} / Q_V = 28$ F mAh^{-1}. This plot is applicable when the second and sixth terms in equation 4a are dominant.

The table of contents entry should be 50–60 words long and should be written in the present tense and impersonal style (i.e., avoid we). The text should be different from the abstract text.

TOC entry

Here the tradeoff between areal capacity and rate performance in battery electrodes is explored from both experimental and theoretical standpoints. For thick electrodes, the best tradeoff is achieved when the volumetric capacity, porosity and conductivity of the electrodes is high. Conversely, minimizing solid-state diffusion times is only important for thin electrodes.

Keyword: Performance optimization

Sang-Hoon Park, Ruiyuan Tian, João Coelho, Valeria Nicolosi, Jonathan N Coleman *

Title: Quantifying the trade-off between absolute capacity and rate-performance in battery electrodes

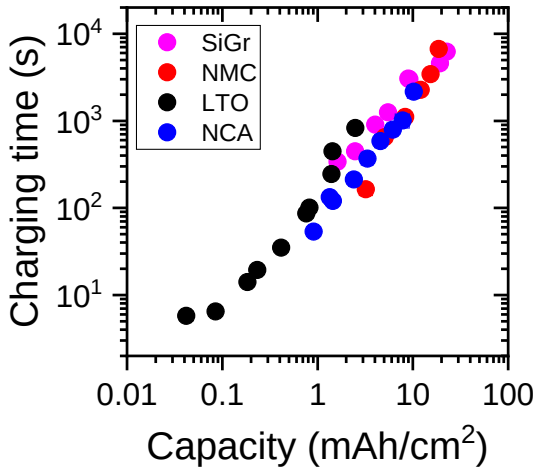

ToC figure ((Please choose one size: 55 mm broad × 50 mm high **or** 110 mm broad × 20 mm high. Please do not use any other dimensions))